Flow Phenomena in Stirred Tanks

Part I. The Impeller Stream

Flow parameters were measured in a baffled, turbulent, stirred tank agitated by a six-blade, disk style turbine. The working fluid was air. Mean and fluctuating velocities were measured between the blades of the impeller with a probe mounted on the spinning impeller. Mean velocities, turbulent velocities, one-dimensional energy spectra, and Eulerian autocorrelation functions were measured in the impeller stream by using the shielded hot-wire anemometer of Gunkel et al. (1971) which permits the measurement of turbulence parameters in flows of very high turbulence intensity. Reliable impeller pumping capacities were obtained yielding $Q_{rad}/ND^3 = 1.0$ at the impeller periphery. An energy balance on a control volume containing the impeller and the impeller stream showed that the energy put into the tank via the impeller appeared as a net efflux of kinetic energy leaving the control volume. Therefore, most of the energy input to the tank is dissipated in the bulk of the tank.

ALFRED A. GÜNKEL and MARTIN E. WEBER

Department of Chemical Engineering
McGill University
Montreal, Quebec

SCOPE

No progress in the understanding of mixing operations in stirred tanks can be achieved without a better picture of the flow phenomena in stirred tanks. The main objectives of this study were: to measure flow parameters in a turbulent stirred tank, from them to determine how the energy put into the tank was dissipated, and then to derive theoretically supported scale-up procedures for operations in stirred tanks. The achievement of this last objective is of most immediate importance for practical applications.

Previous studies on the flow phenomena in the impeller stream of a stirred tank have reported mean velocities, turbulent velocities, one-dimensional energy spectra, and correlation functions (Kim and Manning, 1964; Bowers, 1965; Cutter, 1966; Sato et al., 1967; Mujumdar et al., 1970; Rao and Brodkey, 1972; Cho et al., 1971). The main shortcoming of these studies is the poor precision of the experimental techniques which were not suitable for the high turbulence intensities (up to 50%) found in stirred tanks. Nevertheless, Cutter (1966) concluded that 70% of the energy put into the tank was dissipated within the impeller and the impeller stream, and only 30% was dissipated in the bulk of the tank. In the first part of the present paper, accurate flow parameters are reported in the impeller stream from a six-blade, disk style turbine. An energy balance is then used to determine the amount of energy dissipated in the impeller and the impeller stream.

CONCLUSIONS AND SIGNIFICANCE

A very complete picture of the flow pattern in the neighborhood of a six-blade, disk style turbine impeller has been obtained. For the first time velocities between the blades of a rotating impeller have been measured. These measurements indicated that four vortices are present between each pair of blades, two above and two below the disk.

Mean velocity profiles in the impeller stream showed a jet like behavior, with the impeller stream entraining fluid as it traveled from the periphery of the impeller to the tank wall. Integration of the velocity profiles yielded impeller pumping capacities.

The normalized one-dimensional energy spectra were the same everywhere in the impeller stream and for all operating conditions. The spectra had a slope of $-5/3$ over about 1.5 decades of the frequency space. In the high frequency range the slope was about -7. The spectra taken close to the impeller tip showed a peak corresponding to the frequency of the passing impeller blades and a second smaller peak corresponding to twice that frequency owing to the presence of the vortices between the blades. The Eulerian autocorrelations confirmed the periodic character of the flow in the impeller stream close to the impeller.

From an energy balance it was found that most of the energy transmitted into the tank was dissipated outside the impeller stream, that is, in the bulk of the tank. Here the turbulence intensity is high, and dissipation is through a turbulent mechanism. In the high wave number range the turbulence is isotropic and, following Kolmogoroff, depends only upon the energy dissipation per unit mass and the kinematic viscosity. This explains why relationships involving energy dissipation per unit volume or per unit mass within the tank have been so successful in correlating some phenomena in stirred tanks.

Correspondence concerning this paper should be addressed to M. E. Weber. A. Günkel is with Canadian Industries Limited, McMasterville, Quebec.

PREVIOUS WORK

Turbulent flow parameters in the discharge stream of an impeller in a stirred tank have been measured by several methods: by using a pressure transducer (Kim and Manning, 1964), a hot wire anemometer (Bowers, 1965; Sato et al., 1967; Mujumdar et al., 1970), a hot film anemometer (Cho et al., 1971; Rao and Brodkey, 1972), and photography of tracer particles (Cutter, 1966; Komasawa et al., 1974). All studies were with water as the working fluid except that of Mujumdar et al. (1970) who used air. The accuracy of all of these data is uncertain owing to the large fluctuating velocity component present in the flow. A detailed evaluation of all of these methods has been presented elsewhere (Günkel, 1973). Only qualitative data (Van't Riet and Smith, 1973) have been taken between the blades of a rotating, disk style turbine.

Cutter (1966) attempted to determine where within the tank the energy transmitted by the impeller was dissipated. Using the mechanical energy balance, he deduced that approximately 20% of the energy was dissipated within the confines of the impeller, 50% was dissipated within the impeller stream, and 30% was dissipated in the remainder of the tank. The reliability of these figures is, however, strongly dependent upon the accuracy of the velocity data, since the flux of kinetic energy across a control surface is proportional to the cube of the velocity.

APPARATUS AND EXPERIMENTAL TECHNIQUE

The design and the dimensions of the tank and impeller used in this study are shown in Figure 1. The tank was made of plexiglass. A section of the tank wall between two baffles was removed, the gap being covered by a shell which could be turned around the tank axis. The flowmeters which were mounted on this shell could reach one quarter of the tank. Provision was also made to insert the flowmeters through the top cover of the tank. The impeller, a standard six-blade, disk style turbine impeller with $w/D = 0.2$ and $l/D = 0.25$, was mounted midway between the top cover and the bottom of the tank. The tank diameter and height were 45.7 cm. The impeller diameter was 22.8 cm. Also shown in Figure 1 are the coordinate system and the notation used in this study. The origin of the angular coordinate γ is halfway between two baffles. The radial coordinate r has its origin at the tank axis. A second radial coordinate s has its origin at the impeller tip. The velocity U_{res} is the vector sum of the radial and tangential velocity components in a horizontal plane.

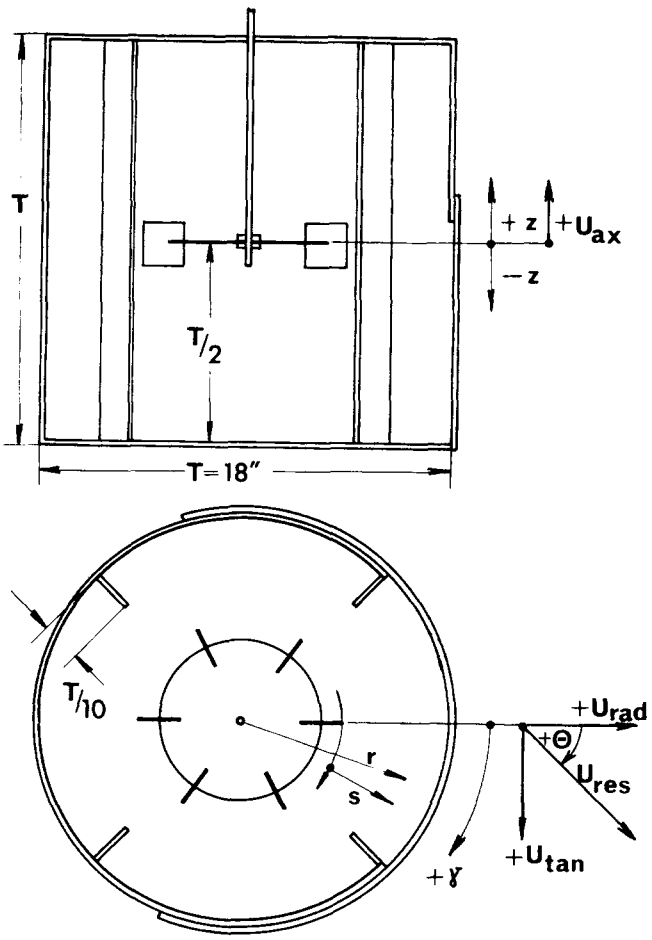

Fig. 1. Tank and impeller system with coordinates.

Most of the data in the impeller stream were obtained by using the shielded hot-wire anemometer described by Günkel et al. (1971). This probe, which incorporates two separate hot wires, can detect flow reversals and produces both positive and negative voltage signals depending upon the direction of the instantaneous velocity. The particular configuration used here is given in Figure 3 of the paper by Günkel et al. (1971). Advantage was taken of the fact that the shielded probe follows the cosine law (see Figure 10 of Günkel et al., 1971). The flow direction was determined by rotating the probe about its axis in increments of 10 deg. over 180 deg. The maximum in a cosine curve fitted to the points gave the flow direction. The flow directions obtained by this procedure were reproducible within ±1 deg. Some flow directions were also taken with a yaw tube.

Data between the impeller blades were obtained by using a standard hot-wire anemometer. The wire was mounted on the rotating impeller in such a way that the supports were downstream from the wire. The signals from the wire were transmitted by using a mercury contact. The design of the support and the transmission device are given by Günkel (1973).

The working fluid was air. Justification for its use in studies of this sort is given by Mujumdar et al. (1970).

EXPERIMENTAL RESULTS

The Flow Between the Impeller Blades

The velocities between the blades of the rotating impeller were measured by using a standard, single, hot-wire anemometer. The wire was located at $r = 10.4$ cm away from the axis of rotation of the impeller, that is, at 1 cm inward from the impeller tip. The data were taken at $z = 0$ where, for reasons of symmetry, the axial velocity vanishes. The experimental results are presented in Figure 2 as a function of the arc length l_b on the circle with radius $r = 10.4$ cm. The total arc length on this circle between two blades of the impeller is 11 cm. The origin of the coordinate l_b was arbitrarily put at the face of the trailing blade. In order to reach the extreme position of $l_b = 11$ cm, the hot wire was moved in direction of the rotation of the impeller up to the rear face of the leading blade.

By placing the hot wire in a horizontal plane, the wire senses essentially only the radial velocity, while when oriented vertically the wire senses the vector sum of the radial and tangential velocities. This vector sum is called hereafter the *resultant velocity*. By making traverses with these two orientations, it was possible to obtain the radial and tangential velocities. The direction of the tangential velocity relative to the rotating impeller was determined by using a slanted wire. In Figure 2 the velocities have been normalized with respect to the velocity of the impeller tip. It should be noted that the velocities in the

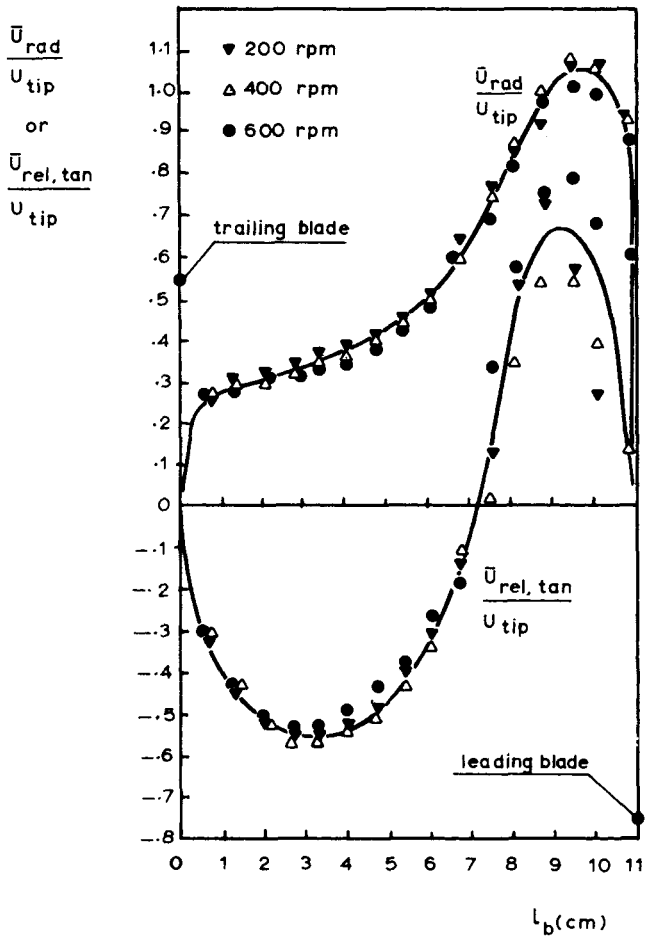

Fig. 2. Tangential and radial components of the mean velocity measured between the impeller blades.

figure are given relative to an observer moving with the hot wire. Since the probe itself was moving with a tangential velocity equal to U_{cir}, to obtain the tangential velocity relative to a stationary observer U_{cir} must be added to U_{tan}. For this set of measurements $U_{cir}/U_{tip} = 0.91$.

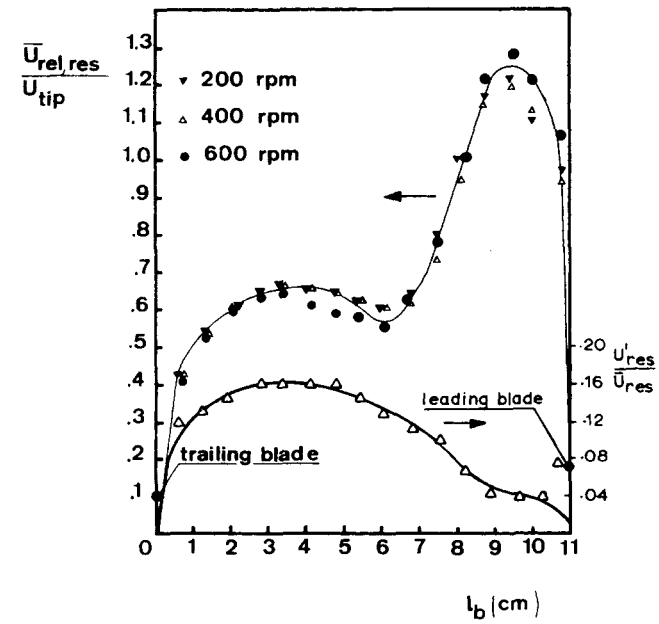

Fig. 3. Resultant mean velocity and rms turbulence velocity in the direction of the resultant velocity.

The data show a large radial flow outward behind the leading blade with lower radial velocities ahead of the trailing blade. The tangential velocity is zero some distance behind the leading blade with flow toward the leading and trailing blades on either size of the zero crossing. Relative to a stationary observer the tangential velocity is always in the direction of rotation of the impeller. Figure 3 presents the mean resultant velocity relative to a moving observer and the turbulence intensity relative to a stationary observer. The root-mean-square fluctuating velocity did not vary significantly, while the intensity of turbulence varied from 4 to 16% due mainly to the variation in the local mean velocity. The high turbulence intensity measured by many other workers with a stationary probe in the impeller stream near the impeller tip is due to vortex shedding from the impeller blades and is not a random turbulence. This was first noted by Mujumdar et al. (1970).

Consideration of the data taken here and those in the flow entering the impeller (discussed in the next section) gives the qualitative picture of the flow within the confines of the impeller sketched in Figure 4 relative to an observer moving with the impeller. This observer will sense a velocity vector U_{ent} as the flow enters the impeller. The flow will then form four vortices. The smaller vortex behind the leading blade has a larger radial velocity as shown in Figure 2. Van't Riet and Smith (1973) have also detected the strong vortex behind the leading blade. The details of the flow at the top and bottom edges of the blade are certainly more complex than sketched in Figure 4, but the pattern near $z = 0$ is well supported.

Spatial averages of U_{rad} and U_{tan} were taken along the arc length l_b. These averages should be consistent with time averages seen by a stationary observer located at $z = 0$ and close to the impeller tip. As seen in the next section, there is good agreement between the data taken between the impeller blades and the data taken in the impeller stream.

Mean Velocities in the Impeller Stream

Figure 5 represents the axial velocities and the directions of the flow entering the impeller stream and the impeller itself. The data were taken at $z = -3.75$ cm, that is, 1.47 cm below the bottom of the impeller blade where the radial velocity was negligible. Figure 6 shows the mean resultant velocity for several radial stations as a function of vertical distance. The impeller flow is jet-like, with a decreasing center-line velocity and entrainment expanding the jet. The resultant center-line velocity at the impeller

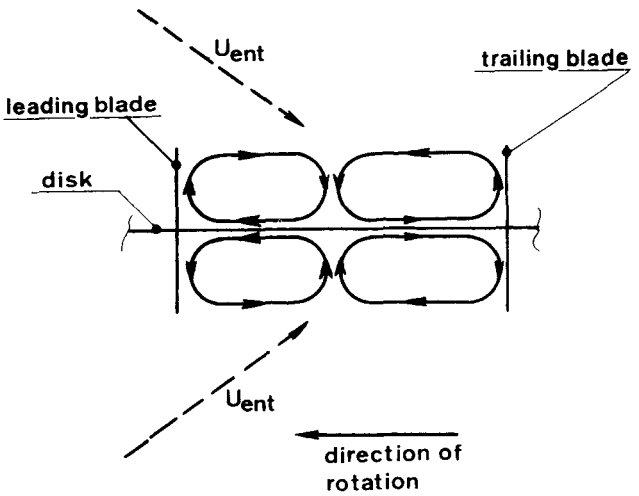

Fig. 4. Sketch of the vortex flow pattern between the impeller blades.

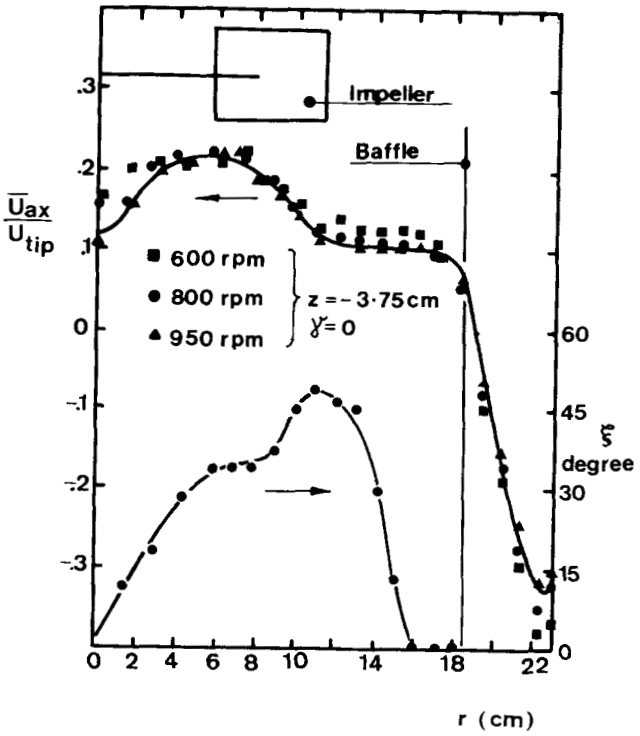

Fig. 5. Mean axial velocity and angle of flow as a function of radial position.

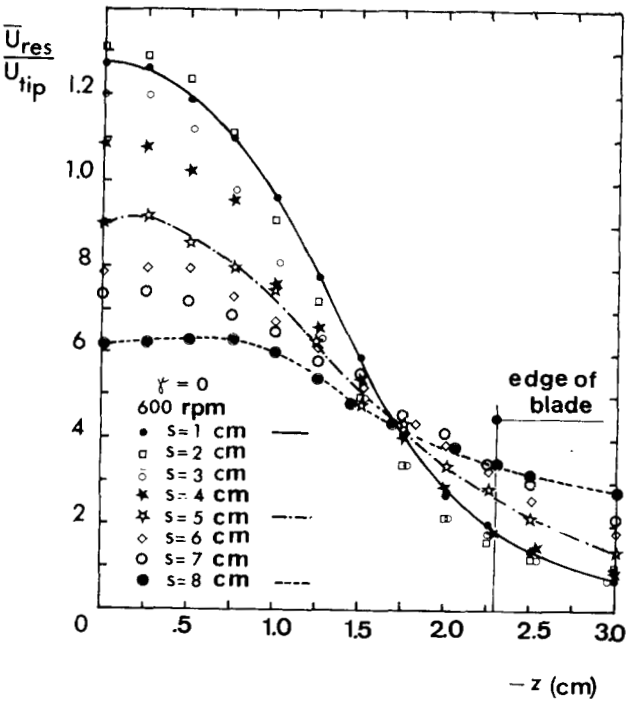

Fig. 6. Profile of the mean resultant velocity in the impeller stream at different radial positions.

tip is about 1.2 times the tip velocity. The same value was obtained in water by Cutter (1966) using the photographic technique. Values about 20% lower were found by Cho et al. (1971) using a hot-film anemometer and by Rao (1969) working with an open style impeller and using a yaw tube. Rao's hot-film data are much lower and are probably in error. Center-line velocities in component form are plotted in Figure 7. The two points for $s < 0$ were obtained by space averaging the data taken from the

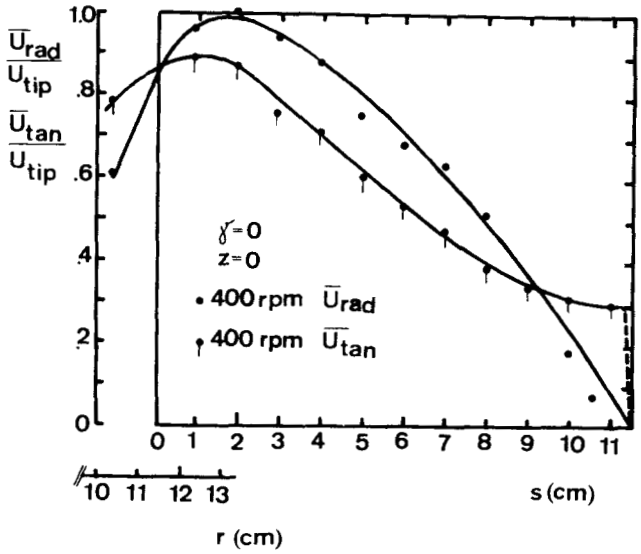

Fig. 7. Radial and tangential components of the mean velocity at the center line of the impeller stream.

hot wire mounted on the spinning impeller. In the impeller center line, the velocity components reach maxima a small distance from the impeller tip. The mean radial velocity in the center line of the impeller stream and close to the impeller tip measured in this study was about 0.8 times the impeller tip velocity. The same result is reported by Kim and Manning (1964) using a pressure transducer probe, again by Cutter (1966) and by Mujumdar et al. (1970) using a standard hot-wire anemometer. For comparison, data were also taken in the impeller stream center line with a single, unshielded, hot-wire anemometer and a yaw tube. The resultant velocities from these instruments were 10 to 20% lower than those from the shielded probe near the impeller tip. The yaw tube, however, gave flow angles in agreement with those from the shielded probe, thus supporting the hypothesis of Rao and Brodkey (1972) that the yaw tube can be used to determine flow direction in the impeller stream.

Turbulent Velocities in the Impeller Stream

The turbulent velocity near the impeller tip is shown in Figure 8, where the root-mean-square value of the turbulent velocity (in the direction of the resultant velocity) is plotted against vertical distance. The normalizing velocity is the resultant velocity at the impeller center line. Near the impeller tip the fluctuating velocity has a large periodic component due to the passage of the blades. Measurements between the impeller blades showed that the root-mean-square fluctuating velocity was nearly independent of position between the impeller blades. This suggests that the periodic and random fluctuations were uncorrelated; that is

$$\overline{u^2}_{res} = \overline{u^2}_{res(per)} + \overline{u^2}_{res(ran)} \qquad (1)$$

The value of $\overline{u^2}_{res}$ was obtained directly from the root-mean-square output of the shielded hot-wire probe. The frequency of the periodic component is Nn_b. The contribution at this frequency was obtained by sending the signal from the shielded probe through the narrow band filter of the wave analyzer tuned to the frequency of the periodic component, thus giving $\overline{u^2}_{res(per)}$. The random component, $\overline{u^2}_{res(ran)}$ was calculated from Equation (1). These components are plotted in Figure 8. At the center of the impeller stream the root-mean-square value of the fluctuations is about 30%, with the major contribution

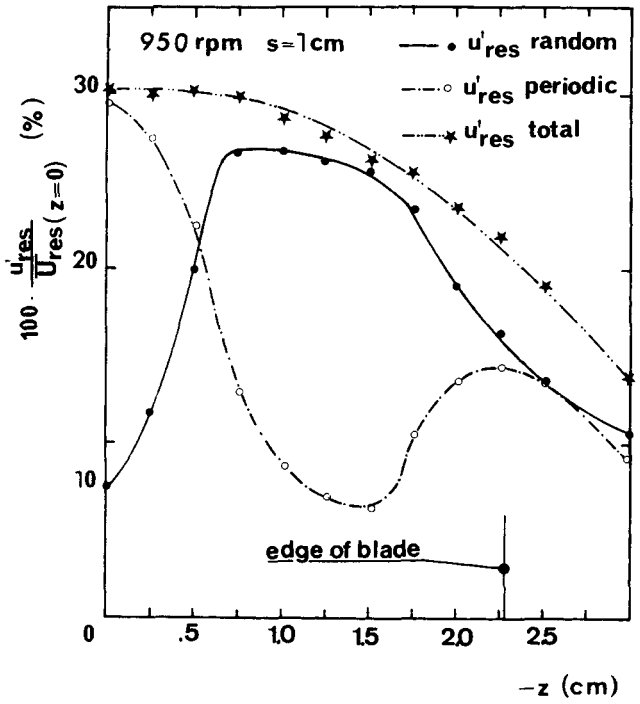

Fig. 8. Profile of the turbulence intensity in the impeller stream close to the tip of the impeller.

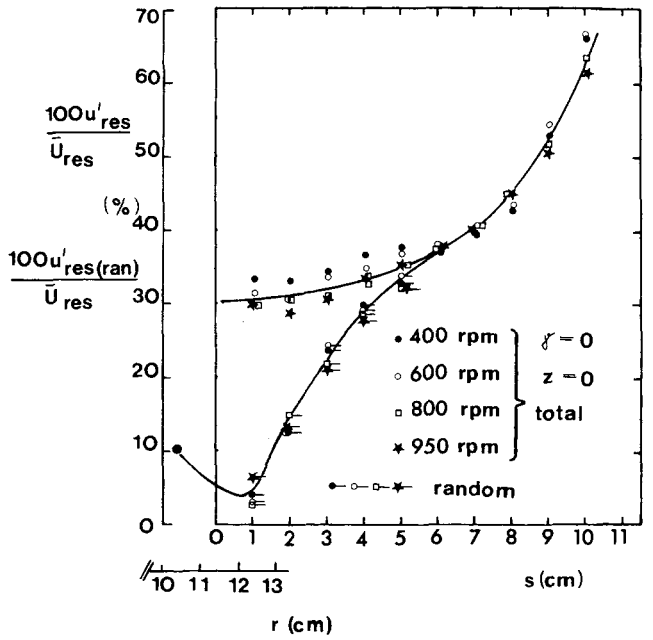

Fig. 9. Total and random turbulence intensity in the direction of the resultant velocity at the impeller center line.

due to the periodic passage of the impeller blades. The truely random fluctuations are rather small, in agreement with the data taken between the rotating blades. Towards the edge of the blades the random fluctuations become much more important, perhaps due to the vortex structure noted earlier.

If the value of u'_{res} were normalized with the local value of $\overline{U}_{res}$ to form a local turbulence intensity, this intensity would increase from 30% at the impeller center line to over 100% at the edge of the impeller blade. Such large intensities can be accurately measured only by an instrument like that used here which responds to changes in flow direction.

Figure 9 shows the change in the intensity of turbulence

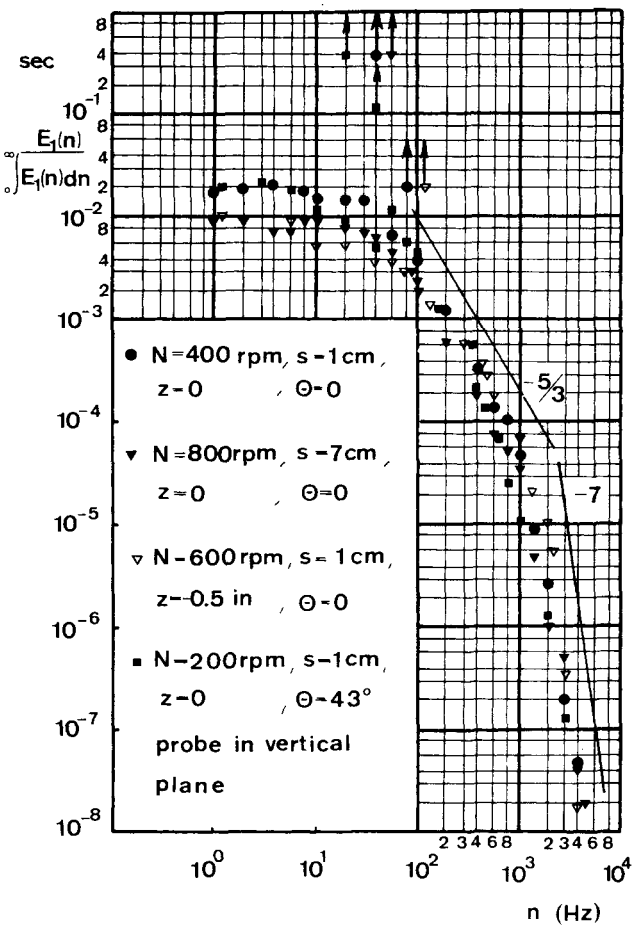

Fig. 10. One dimensional energy spectra in the impeller stream.

at the center line of the impeller stream as a function of radial position. The random contribution has been separated from the total as before. For distances larger than 6 cm from the tip of the blades, the periodic fluctuations have disappeared, and only random turbulence remains. Near the impeller, however, the periodic fluctuations are much larger than the random fluctuations. The points for $s < 0$ were obtained from the data taken within the rotating impeller blades by space averaging the fluctuating velocities and by dividing by the resultant velocity relative to a stationary observer. The data in Figure 9 are consistent with those of Mujumdar et al. (1970) who also separated the velocity fluctuations into random and periodic components.

Normalized, one-dimensional energy spectra obtained in the impeller stream are shown in Figure 10. The spectra were taken with the probe normal to the local mean velocity vector. Close to the impeller tip a peak corresponding to the frequency of the passing impeller blades was observed as well as a second, smaller peak corresponding to twice that frequency. The occurrence of the second peak is to be expected in view of the structure of the flow between the impeller blades which shows two maxima in resultant velocity. Away from the impeller tip the peaks in the energy spectra quickly disappeared as the periodic fluctuations decayed. The spectra were normalized by using the integral value of $\int_0^\infty E_1(n)dn$, omitting the contribution of the periodic velocity fluctuations. The normalized energy spectra coincided for all operating conditions and locations throughout the impeller stream within the precision of the experimental technique. The

TABLE 1. MASS BALANCE AROUND IMPELLER
Pumping capacity, m^3/s

N, s^{-1}	$z = 3.75$ cm Q_{rad}	$s = 1$ cm Q_{ax}	$z = 3.75$ cm Q_{rad}	$s = 7$ cm Q_{ax}
6.7	0.083	0.086	0.164	—
10.0	0.123	0.122	0.215	0.215
13.3	0.154	0.157	0.270	0.260

TABLE 2. ENERGY BALANCE AROUND IMPELLER
Kinetic energy flux, $kg\ m^2/s^3$

N, s^{-1}	Reynolds number $Re \times 10^{-4}$	Control surface 1	Control surface 2	Total	Power number N_p
6.7	1.46	1.58	0.21	1.37	6.1
10.0	2.20	3.93	0.57	3.36	4.5
13.3	2.93	7.94	1.17	6.77	3.8

spectra show three distinct regions, one with slope zero, one with slope $-5/3$, and one with a slope of about -7. The energy spectra reported in the literature by Kim and Manning (1964), by Mujumdar et al. (1970), by Rao and Brodkey (1972), by Sato et al. (1967, by Cho et al. (1971), and by Komasawa et al. (1974), as well as the concentration spectra reported by Manning and Wilhelm (1963), by Reith (1965), and by Cho et al. (1971), are similar to the spectra obtained here.

The Eulerian autocorrelations obtained in this study were similar to those of Mujumdar et al. (1970). The correlation coefficient near the impeller was periodic for large time delays, thus showing presence of the periodic fluctuating velocity near the impeller. The amplitude of the fluctuation in the correlation coefficient decreased with increasing impeller speed. Away from the tip the periodicity in the correlation coefficient disappeared as the periodic velocity component decayed.

DISCUSSION

Pumping Capacity

The pumping capacity of the impeller was calculated at several radial positions (see Appendix for details). The normalized pumping capacities are presented in Figure 11 as a function of the distance from the impeller tip. The pumping capacity increases with radial distance as fluid is entrained into the impeller stream. The maximum volume of fluid entrained is about 80% of that leaving the impeller. The dimensionless impeller pumping capacity (excluding entrainment) is $Q_{rad}/ND^3 = 1.0$. For the same six-blade turbine in water, Cooper and Wolf (1967) found 0.85 using a yaw tube. This difference is expected, since the yaw tube reads about 20% too low near the impeller tip. Holmes et al. (1964) found a maximum normalized pumping capacity (including entrainment) equal to 1.9 in good agreement with the data in Figure 11.

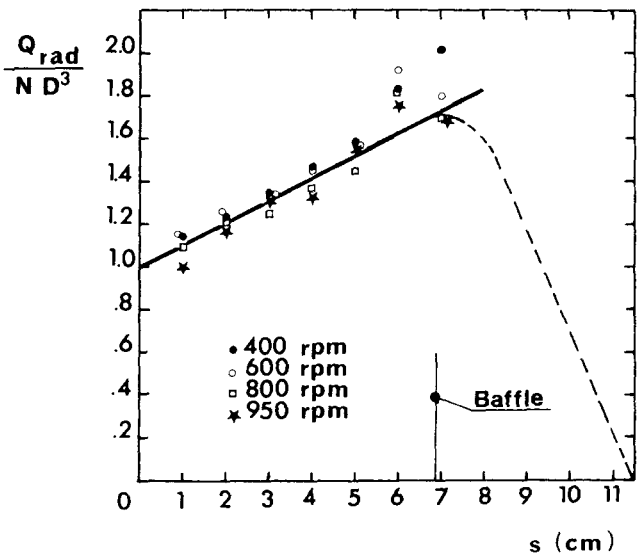

Fig. 11. Profile of the radial pumping capacity of the impeller stream.

Axial pumping capacities (see Appendix) were also computed, and the reliability of the data was tested through the continuity equation [see Equation (A5) in the Appendix]. Table 1 presents axial and radial pumping capacities for two control volumes: one located close to the impeller tip ($s = 1$ cm) and the other located near the baffles ($s = 7$ cm). In all cases, Q_{ax} was within 4% of Q_{rad}. This lends strong support to the reliability of the data, since the axial and radial flows have very different mean velocities and turbulence intensities over the two control surfaces.

Energy Dissipation

The rate of energy dissipation within the impeller stream can be calculated by analyzing a control volume containing the impeller. If there is no energy dissipated within this control volume, the power input to the impeller will equal the net rate of efflux of kinetic energy from the control volume. Details of the equations used to calculate the kinetic energy flux and the simplifications introduced are given in the Appendix.

Table 2 presents the results of these calculations for three impeller rotation speeds. The energy flux entering the impeller stream through control surface 2 is about 15% of that leaving the impeller stream through control surface 1. The last column gives the dimensionless power number calculated from the net rate of efflux of kinetic energy, when no dissipation within the control volume is assumed. Although the power input was not measured in this study, a number of values have been obtained by other workers for $Re > 10^4$, where N_P is constant. For the six-blade, disk style turbine used here, the most reliable values are $N_P = 5.5$ (Calderbank, 1958), $N_P = 5.0$ (Bates et al., 1963) for an open tank, and $N_P = 5.6$-5.8 (Nienow and Miles, 1971) for a tank with a cover.

The calculated power numbers in Table 2 agree well with the literature values. The low value of N_P at the highest impeller speed is the result of consistently low velocity readings for velocities over 10 m/s for the particular probe shield used here [see Figure 10 of Günkel et al. (1971)]. The more accurate data are those at 400 and 600 rev./min. The agreement between the calculated power numbers and those reported in the literature indicates that little of the input energy is dissipated within the confines of the impeller or in the impeller stream. Since the energy put into the tank through the impeller can be accounted for at the exit of the impeller stream, the energy is dissipated in the bulk of the tank. This conclusion disagrees with the view of Cutter (1966) who concluded on the basis of an energy balance that only

30% of the input energy is dissipated in the bulk of the tank. Since the kinetic energy fluxes are obtained by raising measured velocities to the third power, accurate experimental data are necessary in order to obtain reliable fluxes. The data obtained here have low scatter and are the most reliable obtained so far, having been tested for consistency through the mass balance. Cutter's data have sufficient scatter so that reliable kinetic energy fluxes cannot be calculated. Rao and Brodkey (1972) and Komasawa et al. (1974) attempted to measure dissipation rates in the impeller stream and from them to infer whether an appreciable fraction of the input energy was dissipated in the bulk of the tank. Since they used equations valid only for isotropic turbulence and the flow near the impeller is not isotropic, their results are unreliable.

Since most of the energy is dissipated in the bulk of the tank, it is not surprising that correlations based upon the total power input per unit mass or per unit volume work so well for a number of processes in stirred tanks. Notable examples are the correlations of Brian et al. (1969) for mass transfer to suspended solids, Robinson and Wilke (1970) for mass transfer coefficients and interfacial areas in gas-liquid dispersions, and Weinstein and Treybal (1973) for drop size and holdup in liquid-liquid dispersions.

NOTATION

D = impeller diameter
$d\bar{A}$ = unit area vector
$E_1(n)$ = one-dimensional energy spectrum in the frequency space
e_v = rate of energy dissipation inside the control volume
l = length of the impeller blades
l_b = arc length between impeller blades
N = rate of rotation of impeller
N_p = power number $= P/\rho N^3 D^5$
n = frequency
n_b = number of blades on impeller
P = power input
p = pressure
Q_{ax} = axial pumping capacity
Q_{rad} = radial pumping capacity
r = radial coordinate
s = radial coordinate with origin at the impeller tip
T = tank diameter
U = velocity vector
U_i = instantaneous velocity in the i direction
$\overline{U_i}$ = mean velocity in the i direction
u_i = fluctuating velocity in the i direction
u_i' = root-mean-square value of the fluctuating velocity in the i direction
U_{clr} = circumferential velocity of anemometer wire
U_{ent} = velocity of flow entering the impeller
U_{rel} = velocity relative to the impeller
U_{tip} = velocity of impeller tip $= \pi DN$
$u_{res(per)}$ = fluctuating periodic velocity in the impeller stream in a horizontal plane
$u_{res(ran)}$ = fluctuating random velocity in the impeller stream in a horizontal plane
W_{st} = rate of work done by shear stresses on the fluid surrounding the control volume
w = impeller blade width
z = axial coordinate
ϕ = scalar whose gradient is the gravity force vector
ρ = fluid density
$\gamma, \theta, \zeta, \xi$ = angles of the flow direction

Subscripts

ax = axial
res = resultant in a horizontal plane
rad = radial
tan = tangential
1 = control surface 1
2 = control surface 2

LITERATURE CITED

Bates, L. R., L. P. Fondy, and R. R. Corpstein, "An Examination of Some Geometric Parameters of Impeller Power," *Ind. Eng. Chem. Process Design Develop.*, **2**, 310 (1963).

Bowers, R. H., "Some aspects of agitator design," *A.I.Ch.E.-Symposium Series*, **10**, 8 (1965).

Brian, P. L. T., H. B. Hales, and T. K. Sherwood, "Transport of Heat and Mass Between Liquids and Spherical Particles in an Agitated Tank," *AIChE J.*, **15**, 727 (1969).

Calderbank, P. H., "Physical Rate Processes in Industrial Fermentation, Part I: The Interfacial Area in Gas-liquid Contacting with Mechanical Agitation," *Trans. Inst. Chem. Engrs.*, **36**, 443 (1958).

Cho, S. H., P. H. Amarnath, and H. A. Becker, "Turbulence and Mixing in a Stirred Tank," Paper presented at the 21st Canadian Chemical Engineering Conference, Montreal, Canada (Oct., 1971).

Cooper, R. G., and D. Wolf, "Pumping Capacities in Stirred Tanks: Theory and Application," *Can. J. Chem. Eng.*, **45**, 197 (1967).

Cutter, L. S., "Flow and Turbulence in a Stirred Tank," *AIChE.*, **12**, 35 (1966).

Günkel, A. A., R. P. Patel, and M. E. Weber, "A Shielded Hot-Wire Probe for Highly Turbulent Flows and Rapidly Reversing Flows," *Ind. Eng. Chem. Fundamentals*, **10**, 627 (1971).

Günkel, A. A., "Flow Phenomena in Stirred Tanks," Ph.D. thesis, McGill Univ., Montreal, Canada (1973).

Holmes, D. B., R. M. Voncken, and J. A. Dekker, "Fluid Flow in Turbine-Stirred, Baffled Tanks I: Circulation Time," *Chem. Eng. Sci.*, **19**, 201 (1964).

Kim, W. J., and F. S. Manning, "Turbulence Energy and Intensity Spectra in a Baffled, Stirred Tank," *AIChE J.*, **10**, 747 (1964).

Komasawa, I., R. Kuboi, and T. Otake, "Fluid and Particle Motion in Turbulent Dispersion-I: Measurement of Turbulence of Liquid by Continual Pursuit of Tracer Particle Motion," *Chem. Eng. Sci.*, **29**, 641 (1974).

Manning, F. S., and R. H. Wilhelm, "Concentration Fluctuations in a Stirred Baffled Vessel," *AIChE J.*, **9**, 12 (1963).

Mujumdar, A. S., B. Huang, D. Wolf, M. E. Weber, and W. J. M. Douglas, "Turbulence Parameters in a Stirred Tank," *Can. J. Chem. Eng.*, **48**, 475 (1970).

Nienow, A. W., and D. Miles, "Impeller Power Numbers in Closed Vessels," *Ind. Eng. Chem. Process Design Develop.*, **10**, 41 (1971).

Rao, M. A., "Turbulence and Mixing in a Continuous Flow Stirred Tank," Ph.D. thesis, The Ohio State Univ., Columbus (1969).

Rao, A. M., and R. S. Brodkey, "Continuous Flow Stirred Tank Turbulence Parameters in the Impeller Stream," *Chem. Eng. Sci.*, **27**, 137 (1972).

Reith, I. T., "Generation and Decay of Concentration Fluctuations in a Stirred baffled vessel," *A.I.Ch.E.-Symposium Series No. 10*, 14 (1965).

Robinson, C. W., and C. R. Wilke, "Mass Transfer Coefficients and Interfacial Area for Gas Absorption by Agitated Aqueous Electrolyte Solutions," "Chemeca 70," Session 6B, 65, 1970.

Sato, Y., Y. Horie, M. Kamiwano, and K. Yamamoto, "Turbulence Flow in a Stirred Vessel," *Kagaku Kogaku*, **31**, 79 (1967).

Weinstein, B., and R. E. Treybal, "Liquid-Liquid Contacting in Unbaffled Agitated Vessels," *AIChE J.*, **19**, 304 (1973).

Whitaker, S., *Introduction to Fluid Mechanics* Section 7.3, Prentice-Hall, Englewood Cliffs, N.J. (1968).

Van't Riet, K., and J. M. Smith, "The Behaviour of Gas-Liquid Mixtures Near Rushton Turbine Blades," *Chem. Eng. Sci.*, **28**, 1031 (1973).

APPENDIX

The control surface used for calculating the pumping capacity and the energy flux is shown in Figure A1.

Continuity Equation

For constant density the time averaged continuity equation becomes

$$\int\int U \cdot dA = 0 \tag{A1}$$

In terms of the surfaces shown in Figure A1 Equation (A1) becomes

$$2\pi r_1 \int_{-z_2}^{z_2} \overline{U}_{\text{rad}}\, dz - 4\pi \int_0^{r_1} r\, \overline{U}_{\text{ax}}\, dr = 0 \tag{A2}$$

where r_1 is the radial coordinate of control surface 1, and z_2 is the axial coordinate of control surface 2. Identifying the first term as the radial pumping capacity and the second term as the axial pumping capacity, we get

$$Q_{\text{rad}} = 2\pi r_1 \int_{-z_2}^{z_2} \overline{U}_{\text{rad}}\, dz \tag{A3}$$

$$Q_{\text{ax}} = 4\pi \int_0^{r_1} r\, \overline{U}_{\text{ax}}\, dr \tag{A4}$$

and

$$Q_{\text{rad}} = Q_{\text{ax}} \tag{A5}$$

The pumping capacities in Table 1 were evaluated for values of r_1 corresponding to $s = 1$ and $s = 7$ cm In all cases control surface 2 was located at $z_2 = 3.75$ cm, where $\overline{U}_{\text{rad}}$ was negligible.

Energy Equation

Whitaker (1968) has derived the macroscopic mechanical energy balance from the Navier-Stokes equations and has applied it to a control volume with moving boundaries. Taking a fluid control volume surrounding the impeller and noting that the impeller forms a moving boundary of the control volume, Whitaker's equation (7.3-27) can be rearranged to the following form after time averaging.

$$\overline{P} = \rho \int\int_{A_1} \frac{|U|^2}{z} + \phi + \frac{P}{\rho}(\overline{U} \cdot d\overline{A}) + W_{st} + e_v \tag{A6}$$

P is the power transmitted into the control volume, e_v is the rate of energy dissipation inside the control volume, and W_{st} is the rate of work done by the shear stresses on the fluid surrounding the control volume. In deriving Equation (A6), the gravity force has been written as the gradient of the scalar ϕ.

It can be shown that the work done by the normal stresses and the flux of potential energy can be neglected (Günkel, 1973). Likewise, the work done by the shear stresses can be neglected in the fully turbulent range because the power input is not a function of the Reynolds number. Hence, Equation (A6) can be simplified to give

$$\overline{P} = \rho \int\int \frac{|U|^2}{2}(\overline{U} \cdot d\overline{A}) + e_v \tag{A7}$$

The integral term represents the net efflux of kinetic energy from the control volume.

The flux of kinetic energy is computed separately for control surfaces 1 and 2 of the control volume shown in Figure A1. The instantaneous velocity vector at control surface 1 is

$$|U| = \sqrt{(\overline{U}_{\text{res}} + u_{\text{res}})^2 + u^2_{n,\text{res}} + (\overline{U}_{\text{ax}} + u_{\text{ax}})^2} \tag{A8}$$

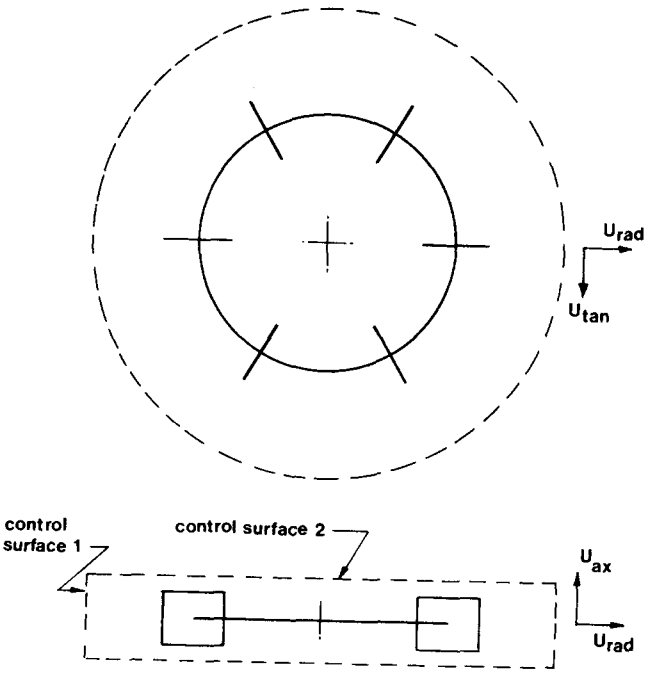

Fig. A1. Control surfaces used in calculating the pumping capacity and the flux of kinetic energy.

where $\overline{U}_{\text{res}}$ is the mean velocity in a horizontal plane, and $u_{n,\text{res}}$ is the fluctuating velocity normal to $\overline{U}_{\text{res}}$ in a horizontal plane.

For control surface 1

$$(U \cdot dA) = |U| \cos\theta \cos\xi\, 2\pi r\, dz \tag{A9}$$

and

$$\cos\theta = \cos(\overline{\theta} + \theta') = \cos\overline{\theta}\cos\theta' - \sin\overline{\theta}\sin\theta' \tag{A10}$$

$$\cos\theta' = \frac{\overline{U}_{\text{res}} + u_{\text{res}}}{\sqrt{(U_{\text{res}} + u_{\text{res}})^2 + u^2_{n,\text{res}}}} \tag{A11}$$

$$\sin\theta' = \frac{u_{n,\text{res}}}{\sqrt{(U_{\text{res}} + u_{\text{res}})^2 + u^2_{n,\text{res}}}} \tag{A12}$$

$$\cos\xi = \frac{\sqrt{(\overline{U}_{\text{res}} + u_{\text{res}})^2 + u^2_{n,\text{res}}}}{\sqrt{(U_{\text{res}} + u_{\text{res}})^2 + u^2_{n,\text{res}} + (U_{\text{ax}} + u_{\text{ax}})^2}} \tag{A13}$$

where the angles are shown in Figure A2.

$$I_1 = \pi r_1 \rho \int_{-z_2}^{z_2} \overline{(U_{\text{res}} + u_{\text{res}})^2 + u^2_{n,\text{res}} + (U_{\text{ax}} + u_{\text{ax}})^2}\,[(\cos\theta\,(U_{\text{res}} + u_{\text{res}}) - \sin\theta\, u_{n,\text{res}}]dz \tag{A14}$$

For control surface 1, the integral in Equation (A7) can now be written as

where I_1 is the flux of kinetic energy through control surface 1.

If all the variables including the double and triple correlations are known as functions of z, the above expression could be evaluated. Although $\overline{U}_{\text{ax}}$ and u_{ax} were not measured in the impeller stream, some approximations can be made. For reasons of symmetry, $\overline{U}_{\text{ax}}$ is zero in the center line of the impeller stream ($z = 0$). It was found by doing a traverse at $z = -3.75$ cm that $\overline{U}_{\text{ax}}$ is zero at $r \approx 18$ cm (Figure 5). Therefore, it was assumed that $\overline{U}_{\text{ax}}$ was negligible in the impeller stream at $s = 7$ cm ($r = 18.4$ cm), and thus control surface 1 was located at $s = 7$ cm. In addition, since at $s = 7$ cm the periodic velocity fluctuations have disappeared (Figure 9), it was assumed that the flow was approximately iso-

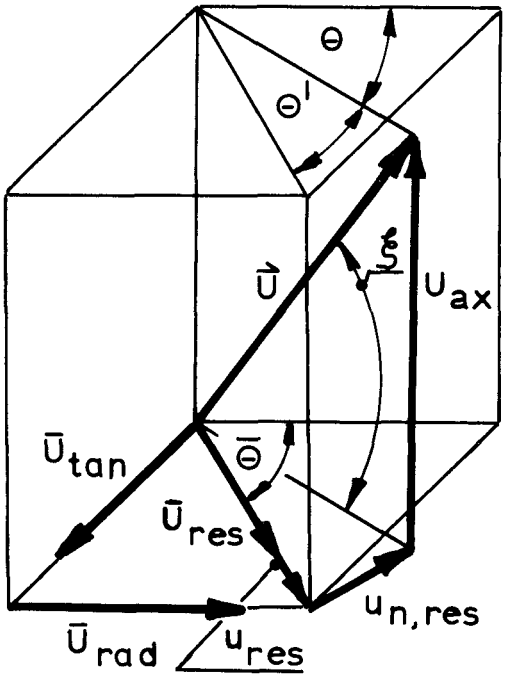

Fig. A2. Velocities and angles used for calculating of the energy flux through control surface 1.

tropic at any z in the impeller stream at $s = 7$ cm:

$$\overline{u^2_{n,\mathrm{res}}} = \overline{u^2_{\mathrm{ax}}} = \overline{u^2_{\mathrm{res}}} \qquad \text{(A15)}$$

Incorporating these simplifications and neglecting fluctuating velocities raised to the power 3, we get

$$I_1 = \pi r_1 \rho \int_{-z_2}^{z_2} [(\overline{U^3_{\mathrm{res}}} + 5\overline{U}_{\mathrm{res}}\,\overline{u^2_{\mathrm{res}}}) \cos\overline{\theta} - 2\overline{U}_{\mathrm{res}}\,\overline{u^2_{\mathrm{res}}} \sin\overline{\theta}]\, dz \qquad \text{(A16)}$$

The flux of kinetic energy through control surface 2 was determined similarly by assuming that $\overline{U}_{\mathrm{rad}}$ was negligible and that the flow was isotropic:

$$I_2 = 2\pi\rho \int_0^{r_1} [(\overline{U^3}_{\mathrm{res},at} + 5\overline{U}_{\mathrm{res},at}\,\overline{u^2}_{\mathrm{res},at}) \cos\overline{\zeta} - 2\overline{U}_{\mathrm{res},at}\,\overline{u^2}_{\mathrm{res},at} \sin\overline{\zeta}]\, r dr \qquad \text{(A17)}$$

$\overline{U}_{\mathrm{res},at}$ is the sum of the velocity components $\overline{U}_{\mathrm{ax}}$ and $\overline{U}_{\mathrm{tan}}$, and $u_{\mathrm{res},at}$ is the fluctuating velocity in direction of $\overline{U}_{\mathrm{res},at}$. The angles and velocity components are shown in Figure A3.

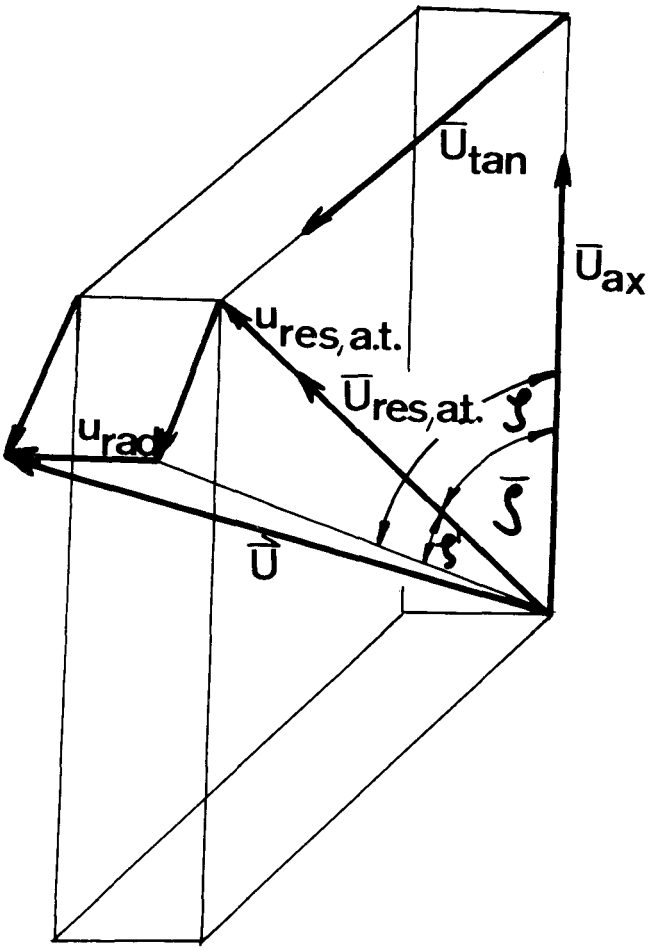

Fig. A3. Velocities and angles used for calculating the energy flux through control surface 2.

All the terms in Equations (A16) and (A17) were obtained from measured velocities. The control surfaces were set at $s = 7$ cm and $z_2 = \pm 3.75$ cm for the data presented in Table 2.

Manuscript received June 10, 1974; revision received and accepted April 30, 1975.

Part II. The Bulk of the Tank

Turbulence parameters were measured in the bulk of turbulent stirred tanks of 45.7 and 91.4 cm diameter with air as the working fluid. Three types of turbine impellers were studied ranging in diameter from 22.8 to 45.7 cm. The turbulence in the bulk of the tank was essentially homogeneous and isotropic. The normalized one-dimensional energy spectra and the Eulerian autocorrelation functions were approximately the same throughout the tank and for all tanks, impellers, and operating conditions. The space averaged turbulent velocities were correlated by using the turbulent energy equation. A transformation of the measured spectra from the frequency space to the wave number space was accomplished. Integration of the dissipation spectra in the wave number space confirmed that most of the energy input is dissipated in the bulk of the tank through the turbulent motion. The results were extended to low viscosity liquid systems and used to interpret the data on mass transfer from suspended particles.